COMPARISON OF THE MSC/NASTRAN AND HOLOGRAPHIC INTERFEROMETRY DATA ON A LOCAL STRAIN/STRESS EVALUATION IN THE ELASTO-PLASTIC RANGE

A.S. DZUBA, V.D. GRIGORIEV, V.S. PISAREV

Moscow Institute of Physics and Technology
Educational Scientific Experimental Centre
16, Gagarina str., Zhukovsky, Moscow reg., 140160 Russia

ABSTRACT

The report presented is related to the MSC/NASTRAN implementation to an accurate determination of a stress/strain concentration both in the elastic and elasto-plastic deformation range. This problem is of great importance from a low-cyclic-fatigue life-time prediction point of view.

The elastic stress concentration problem in a thin plane specimen under tension and thin-walled curved circular cylindrical shell subjected to torsion are considered carefully through the use of the Version 68.1. The accuracy of numerical results in both cases is established by comparing them with the corresponding experimental data obtained by means of holographic interferometric measurements. The calculation of maximum stress values is carried out by using QUAD4 Corner Output. An excellent agreement between numerical and experimental results have been revealed.

An evolution of local elasto-plastic strains in a thin plane strip with a circular open hole under static tension is studied. The data of holographic interferometric measurements are used again in order to estimate the accuracy of numerical solution for different levelsof applied external load. An influence of the circumferential strain gradient on results of a maximum elasto-plastic strain calculation is dicussed in detail.

1. INTRODUCTION

The great majority of essential structural elements in different fields of engineering are operating under the conditions of so-called low-cyclic fatigue. Low-cyclic fatigue can be considered as a process characterized by a high level of local elasto-plastic strains arising at irregular zones of the structure under cyclic in-service loading.

Strain or stress concentration is the main reason for the occurance of local elasto-plastic strains. This leads to a decrease in a structure's life-time in accordance with low-cyclic fatigue laws. One of the most typical geometric strain/stress concentrator is a circular hole either open or filled with a cylindrical inclusion.

Promising approaches to a reliable numerical life-time prediction of structural elements and its optimal design from a fatigue strength standpoint should be based on a correct quantitative description of local elasto-plastic strain evolution [1]. But some serious difficulties have to be overcome to establish a reliable analytical or numerical method of quantitative determination of local elasto-plastic strains especially taking into account strain history under cyclic loading [1,2]. The first of them is related to the fact that the deformation trajectories in most points of interest have non-linear character and, sometimes, strain hysteresis loops due to both material plastic properties and a contact interaction character. The second problem resides in the fact that local mecanical properties of the material at irregular zones of structure are being changed under cyclicloading and, generally, cannot be obtained by means of a standard testing unnotched specimens.

It is evident that MSC/NASTRAN contains all essential prerequistes needed for generation of the numerical methods of life-time prediction under low-cyclic fatigue conditions based on detailed local elasto-plastic strain analysis [3,4]. However, in order to reach the final objective with the best results the available computational capabilities should be supplemented with the experemintal data describing a material mechanical behaviour resulted from a non-linear deformation process under cyclic loading. Moreover, the deformation criteria of fatigue crack appearance and growth up to fracture have to be introduced into numerical approaches for correct quantitative representation of differet stages of a low cyclic fatigue process. The set of above-mentioned data can be effectively obtained through the use of the method of holographic interferometry [2].

The main feature of the holographic interferometric techniques is that enable non-contact measurements to be carried out of three-dimentional displacement fields on both a curved and a plane optically rough surface of opaque objects. The strain tensor used in solid mechanics is generally defined through three displacement components of the corresponding object's point [5]. It is significant that a transition from displacement components to strain values can be performed by means of geometrical relations only, without using any hypotheses concerning both the mechanical properties of deformable medium and the deformation character of a structure to be studied. This fact is of great importance from a standpoint of holographic interferometry implementation to a verification of various numerical strain/stress analysis techniques, since the displacement vector components represent the physical values which can be directly measured on the object surface with a high accuracy.

The main advantage of using holographic methods in experimental mechanics is also exemplified by the ability to measure three-dimensional real rough surface displacement fields without any optical signal converters such as moire' gratings,

whose properties depend on plastic strain values and the number of loading cycles. This provides the unique possibility of investigating elasto-plastic strain fields and the mechanical behaviour of structural materials under cyclic loading, including a crack detection and a crack growth process up to fracture.

The main objective of this study is to make the first step for the implementation of the MSC/NASTRAN to a low-cyclic fatigue life-time prediction based on taking account of local elasto-plastic strain history. This step consists of the verification of concepts on which MSC/NASTRAN calculations of local strains under static loading are founded upon both in elatic and elasto-plastic deformation range.

At first glance it would seem that there are no serious reasons to undertake these studies. As a matter of fact the problem of determination both elastic stress and elasto-plastic strain concentration at zero-half loading cycle has a reliable analytical or numerical solution in many cases. But this is true without doubts for relatively simple problems, such as, for instance, an elastic tension of a finite thin strip with a central circular open hole. Holographic interferometry data are capable to be used for a more refined analysis of a strain/stress concentration problem. Such a refinement is of considerable importance when a low-cyclic fatigue prediction is founded upon a detailed analysis of a local strain evolution at each loading cycle.

Two classical problems were experimentally investigated and data obtained were compared with corresponding results obtained with the MSC/NASTRAN version 68.1.

2. TENSION OF A THIN PLATE WITH AN OPEN HOLE IN AN ELASTO-PLASTIC DEFORMATION RANGE

The first test problem studied represents a thin plane specimen with a central circular open hole subjected to a tension in the elasto-plastic deformation range. A detailed experimental and numerical analysis was carried out for the aluminium (elasticity modulus E = 73000 MPa, Poisson's ratio $\mu = 0.33$) strip of length 260 mm, width 60 mm and thickness 3 mm, with the hole of diameter $2r_0$ = 18 mm. Taking advantage of a symmetry, one forth part of the specimen was used for calculations. This part is shown in Figure 1 with the finite element mesh consisting of the QUAD4 finite elements.

The procedure of reflection hologram recording using an overlay interferometer and the technique used for quantitative interpretation of fringe patterns to obtain the displacement component fields and then the corresponding strain distributions are described in detail in work [2].

The specimen was loaded in the net stress range from zero to the net stress value σ_0 = 232 MPa. The tensile force causing the net stress occurance in the regular cross-sections of the specimen was applied far from the hole in order to avoid the influence of specimen's clamping on the local deformation of the hole vicinity. The whole net stress range is divided into nine loading steps to ensure optimal fringe spacing near the hole at each interferogram to be recorded. The final point of each loading step are 28,60,90,114,142,168,190,208 and 232 MPa.

It should be noted that the last-named value of net stress corresponds to the maximum plastic strain value om the hole edge not less than 1.9×10^{-2} on evidence derived from the standard uniaxial strain vs stress diagram and Neuber formula [1]. This is the first time that this measurement range has been achieved with high accuracy by holographic interferometry.

Typical fringe patterns of plane specimen obtained in the elasto-plastic deformation range for the net stress increment σ_0 from 208 to 222 MPa is shown in Figure 2.

The displacement components were experimentally determined in the nodes of the mesh (see Figure 2) formed by means of the intersection of 9 circle lines of radius r = const (r = 9,11,14,16,19,21,24,27,30 mm) and 16 straight lines φ = const ($D\varphi = \pi/8$ radians) for each loading step.

Some typical experimentally obtained distributions of in-plane Cartesian displacement components u and v along the circle lines r = const are shown in Figure 3 for the net stress increment σ_0 from 208 to 222 MPa. In this Figure the curves with the uneven and even numbers depict the distributions of u and v displacement components, respectively, and curves 1 and 2, 3 and 4, 5 and 6, 7 and 8 correspond to the circle lines r= 9,11, 21,30 mm, respectively.

The experimental displacement conponent distributions along the hole boundary obtained both in the elastic and elasto-plastic deformation range are found to coincide within 3-5 per cent with the corresponding numerical data obtained by the MSC/NASTRAN calculation.

In the case of a load-free circular hole the corresponding elasto-plastic strain and elastic stress components along the hole edge can be expressed as

$$\varepsilon_\varphi = \frac{1}{r_0}\left[\frac{\partial \vartheta}{\partial \varphi}\cos\varphi - \frac{\partial u}{\partial \varphi}\sin\varphi\right] \quad , \qquad \sigma_\varphi = E\varepsilon_\varphi \tag{1}$$

where ε_φ and σ_φ are the circumferential strain and stress, respectively; r_0 is the hole radius; φ is the polar angle ciounting from the coordinate axis x that is directedalong the symmetry axis of the specimen coinciding with the tension direction (see Figure 1); u and v are the Cartesian displacement components of the point belonging to the hole edge, respectively (the y-direction coincides with the other symmetry axis of the specimen); E is the elasticity modulus of the specimen's material.

In the elastic deformation range formulae (1) allow us to estimate the accuracy both of experimental and numerical data obtained through the use of the stress concentration factor K_σ. This value is given by

$$K_\sigma = \frac{\sigma_x^{MAX}}{\sigma_0} \ . \tag{2}$$

where σ_x^{MAX} is derived from the expressions (1) for $\varphi = 90°$; σ_0 is the corresponding net stress increment.

In order to calculate the experimental value of stress concentration factor the discrete sets of two displacement components along the hole edge were approximated in the angular direction with the Fourier series. This allows us to obtain the functional relations needed for following differentiation in accordance with the first expression from (1). The magnitude thus obtained taking into account the expression (2) is K_σ = 3.28. The value of K_σ obtained by means of numerical solving the corresponding elasticity problem is K_σ = 3.30. It should be noted that in the elastic case the MSC/NASTRAN program is capable of calculating the stress values at the nodes of finite element mesh belonging to a hole boundary through the use of QUAD4 Corner Output. The known handbook magnitude of the stress concentration factor in the case involved is equal to 3.36.

All three above-mentioned results are in an excellent agreement that confirms the accuracy and reliability both the experimental and numerical procedure of the elastic local strain/stress determination in a thin notched plane specimen unter plane stress conditions.

Now let us consider the experimental solution of the corresponding elasto-plastic problem. The first expression from (1) can be immediately implemented for a local elasto-plastic strain determination by using holographically obtained displacement components as input data.

Distributions of the circunferential strains ε_φ along the hole edge and 8 circles r = const were obtained by means of Fourier approximation procedure at each loading step. For instance, the distributions of elasto-plastic circumferential strains ε_φ along the hole boundary (curve 1) and the circle line r = 11 mm (curve 2) obtained in accordance with the first relation from (1) and corresponding to Figures 2 and 3 are shown in Figure 4.

The whole set of relations thus obtained allows us to construct the local strain diagram that represents the dependence between maximum local straines ε_x^{MAX} at the root of the notch and the net stresses. This maximum local strain versus net stress diagram obtained through the use of holographic interferometry data is presented in

Figure 5. Note that the values ε_x^{MAX} are derived from **** distributions along the hole edge for $\varphi = 90°$.

The numerical solution of the elasto-plastic problem involved was again carried out with QU•D4 plane finite elements. The uniaxial strain versus stress diagram obtained by a standard way on the unnotched plane specimen in the strain range from zero to 2.3 per cent is used for a quantitative description of the plastic properties of the hardening aluminium alloy in accordance with MSC/NASTRAN Handbook for Nonlinear Analysis, Version 67 (ed. by Sang H.Lee). This diagram is presented in Figure 6. Note the the yield limit value LIMIT1 used in our calculations represents by itself the material proportional limit in tension that is the end point of the linear segment of the corresponding uniaxial strain versus stress diagram. Note, also, that two different numerical solutions were performed by using two yield criteria, namely von Mises and Tresca.

Two calculation procedures consisting of 10 and 100 loading steps before reaching each net stress level coinciding with that used in the course of experimental study were implemented. The standard iteration procedure including five steps per one above-mentioned loading step was used in these two cases. This was done in order to estimate an influence of a loading range discreteness on an accuracy of the final result. It should be pointed out that the values of the total maximum local strain corresponding to each loading level obtained for two different numbers of loading steps coincide to within 3 per cent. This fact is true for each of two yield criteria used.

Typical results of the circumferential strain distribution calculations in the elasto-plastic deformation range corresponding to the net stress increment from 208 to 222 ŒPa are depicted in Figure 4 by curves 3 and 4 for the hole edge and the circle r = 11 mm, respectively. These dependences are obtained through the use of von Mises yield criterion. The corresponding pairs of the experimentally and numerically constructed dependences have almost the same character but some differences in the maximum strain values. The main reason of this resides, evidently, from the fact that the strain magnitudes are calculated inside of the corresponding finite elements as a result of a plastic numerical solution. In the case concerned a considerable mistake in a plastic strain concentration determining arises from a presence of high strain gradient in the radial direction. As a matter of fact the difference between numerical and experimental maximum plastic strain values corresponding to the circle line r = 11 mm is less than that obtained on the hole edge.

In order to more clearly illustrate an influence of the circumferential strain gradient in the radial direction on an accuracy of numerical plastic strain calculation on the hole boundary, the distributions of the total strains in the tension direction along the most loaded specimen's cross-section (x=0) are presented in Figure 7 for the net stress levels 114, 208 and 232 MPa by curve couples 1,2 and 3, respectively. In this Figure the point in the beginning each pair of strain distributions represents the maximum local strain value numerically obtained near the hole boundary.

It is clearly seen that the corresponding experimental and numerical distributions practically coincide one with another starting from the center of the finite element, one boundary of which is situated on the hole edge. Some refinement procedure, like that realized in QUAD4 Corner Output, should be introduced into a numerical plastic strain calculation algorithm on the hole edge in order to reach the corresponding experimentally obtained plastic strain values.

The maximum local strain versus net stress diagram constructed by using numerically obtained data are depicted by curves 2 and 3 in Figure 5 for von Mises and Tresca yield criterion, respectively. The obvious difference between curves 1 and

2 resides from the above-mentioned differences in the experimental and numerical maximum strain magnitudes. Keeping in mind the strain distributions presented in Figure 7, we can argue that von Mises yield criterion gives a better description of a local plastic strain evolution for the hardening aluminium alloy at the zero half loading cycle compared to Tresca criterion.

The total value of the experimentally obtained maximum strain at the root of the notch corresponding to the maximum net stress level σ_0 = 232 MPa is equal 2.2×10^{-2}. In order to estimate the accuracy and reliability of the result obtained, note that this magnitude coincides with Neuber prediction [1] to within 5 per cent.

Thus we can conclude the MSC/NASTRAN is capable of an accurate evaluating local elasto-plastic strains if the maximum strain value calculations would be performed at the mesh nodes being situated on the hole boundary. Note again that for the aluminium alloy involved, having work hardening properties, von Mises yield criterion is preferable.

3. STRESS CONCENTRATION IN A CIRCULAR CYLINDRICAL SHELL WITH AN CIRCULAR CUT-OUT SUBJECTED TO TORSION

The second test problem investigated is related to an elastic stress concentration determination in a curved cylindrical shell with a large size cut-out. A determination of local strains and stresses near irregular zones of thin-walled structures, where all three displacement components are characterized with high gradients in the directions tangential to the object surface, is of great importance from a strength analysis point of view. Analytical methods of stress concentration analysis in curved shells with large size cut-outs often represent a complicated problem [6].

The experimental approach used below for an investigation of local strains and stresses in thin-walled structures is based on three-dimentional displacement field measurements by means of reflection hologram interferometry [2].

The object studied was an aluminium (elasticity modulus E = 72000 MPa, Poisson's ratio μ = 0.33) circular cylindrical shell with a circular open hole subjected to a torsion. The geometrical dimensions of the thin-walled shell are: length L = 320 mm, external radius R = 60 mm, hole radius r_0 = 25 mm, and wall thickness h = 3 mm h/R = 0.05). A diagram of this specimen with the finite element mesh used for numerical solution of the corresponding elastic problem, its clamping and loading scheme are shown in Figure 8.

Reflection holograms that are required to determine the displacement fields along the hole boundary were recorded simultaneously on both the external and interneal faces of the shell. Typical interferogram of the shell obtained for the external face is shown in Figure 9. This fringe pattern corresponds to the torsional moment increment M = 24.5 Nm.

Output information of the holographic experiment in the case involved consists of three displacement component distributions along the hole boundary. If these components are represented in the cylindrical coordinate system, the following expression is valid for the circumferential stress σ_φ distribution along the load-free hole edge on both the external and internalfaces of the shell [6]

$$\sigma_\varphi = \frac{E}{r_0}\left[\frac{\partial \vartheta}{\partial \varphi}\cos\varphi - \frac{\partial u}{\partial \varphi}\sin\varphi\right] + \frac{\varpi \cos^2\varphi}{R} \qquad (3)$$

where u,v are the tangential to the shell face displacement components, with the u-component coincides with the direction of corresponding shell generatrix; w is the normal to the shell surface displacement component; r_0 is the hole radius; φ is the polar angle counting from the shell generatrix passing through the hole center in the anti-clockwise direction; R is the external/internal shell radius; E is the elasticity modulus of shell material.

It is significant that the relation (3) is founded upon the hypothesis of "small" deformation only . This hypothesis is valid in the deformation range corresponding to the sensitivity of holographic interferometer used without doubts. So, an experimental local stress analysis in a curved shell can be carried out without using any hypotheses describing a deformation process of thin-walled structures like Kirchgoff or Reissner-Mindlin hypotheses. Note that such assumpsions have to be introduced into any algorithm on which a numerical stress analysis of thin structural elements are based.

Experimentally obtained distributions of the relative circumferential stress σ_φ/τ_0 (where τ_0 is the net stress increment corresponding to the torsional momemt applied to the free shell end in the course of the experiment) are presented in Figure 10 by curves 1 and 2 for the external and internal faces, respectively. The corresponding data of the MSC/NASTRAN solution are depicted in the same Figure by curves 3 and 4, respectively.

The corresponding pairs of experimental and numerical distributions in Figure 10 are found to agree very closely. Note that the values of elastic circumferential stresses in the case concerned are calculated at the mesh node belonging to the hole edge by making use QUAD4 Corner Output.

In closing we note that the stress distributions presented in Figure 10 are only a part of information resulting from detailed both numerical and experimental study of the hole vicinity deformation. A comparative analysis of the displacement fields and rotation angles of the surface normal reveals some interesting and nonconventional facts and trends. This information should be taken into account in order to ensure a correctness and reliability of a local strain analysis in irregular curved shells in the elasto-plastic deformation range.

4. CONCLUSION

A high accuracy and reliability of the MSC/NASTRAN application to a solution of an elastic stress concentration problem are confirmed for both plane and curved thin-walled structural elements. This follows from a direct comparison of the numerial results obtained and corresponding holographic interferometry data. It should be pointed out that the experimental local stress distribution in a curved circular cylindrical shell with a hole, using for a comparison with corresponding numerical data, is based on the hypothesis of "small" deformation only. This capability of the experimental approach used may be very powerful for a validation of various numerical techniques of local strain/stress analysis in irregular zones of curved thin-walled structures.

A comparative analysis of local strains obtained numerically and experimentally in the elasto-plastic deformation range shows a good coincindence in a character of corresponding dependences but reveals some difference in the maximum plastic strain values resulting from two approaches concerned. This difference makes itself most evident in a high plastic strain gradient zone and increases with the growth of applied load level. The relative difference in the total elasto-plastic strain values obtained experimentally and numerically in accordance with von Mises yield criterion for the maximum net stress level σ_0 = 232 MPa is equal to 20 per cent. The latter magnitude is too large to be acceptable for a correct numerical life-time prediction founded upon detailed local elasto-plastic strain history. Thus, some specific refinement calculation procedure have to be introduced in the MSC/NASTRAN algorithm in order to ensure an accurate determination of plastic strain concentration under static loading and, especially, local elasto-plastic strain evolution under cyclic loading.

Acknowlegments

The authors are most grateful to Mr H.-J. Roesner, Head of MacNeal-Schwendler GmbH Moscow Office whose active and constructive support made this presentation possible.

REFERENCES

1. Collins,J.A.(1981) Failure of Materials in Mechanical Design. Analysis, Prediction, Prevention. John Wiley, New York.

2. Shchepinov,V.P., Pisarev,V.S., Novikov,S.A., et al.(1996) Strain and Stress Analysis by Holographic and Speckle Interferometry. John Wiley, Chichester.

3. Lee,S.H.(ed) MSC/NASTRAN Handbook for Nonlinear Analysis. Version 67.

4. P3/FATIGUE Application Module. User Manual. Publication No.903030, December 1993.

5. Rabotnov,Yu.I.(1979) Mechanics of Solid Deformable Body. Nauka, Moscow.

6. Gus',A.N., Chernyshenko,I.S., Chekhov V.N., et al.(1980) Theory of Thin Shells with Holes. Methods of Shells Calculation, 1. Naukova Dumka, Kiev.@

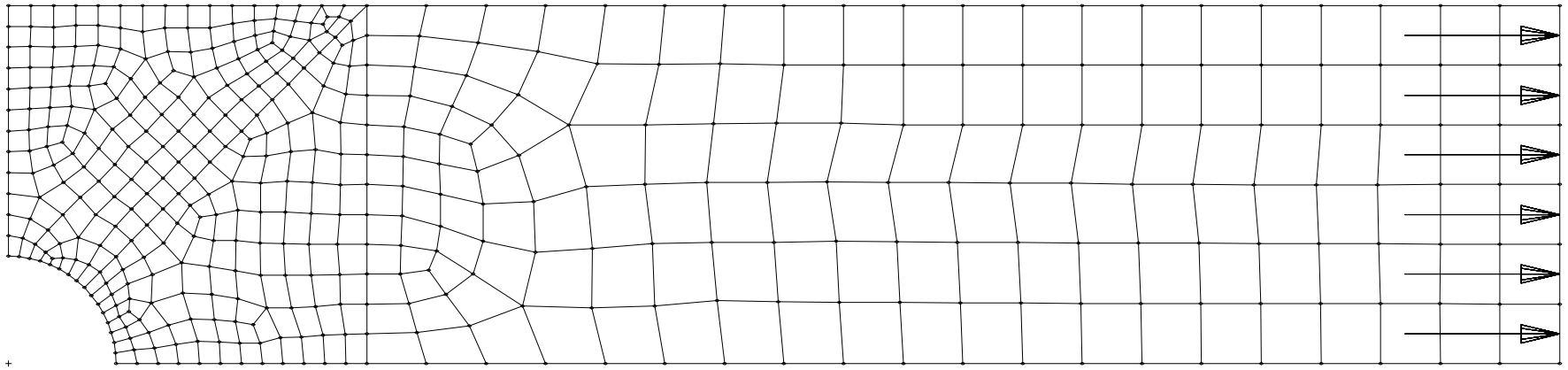

Fig.1 Scheme of the plane specimen with hole and finite element mesh used

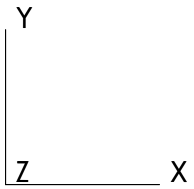

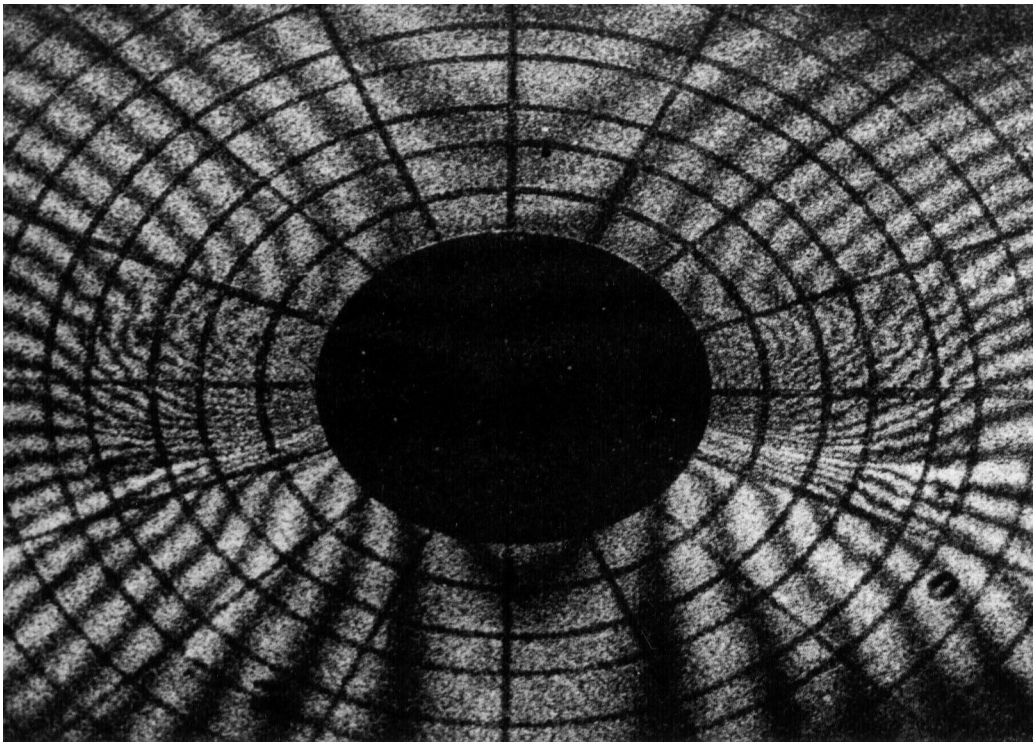

Fig. 2 Interferogram of the plane specimen with hole subjected to a tension in the elasto-plastic deformation range

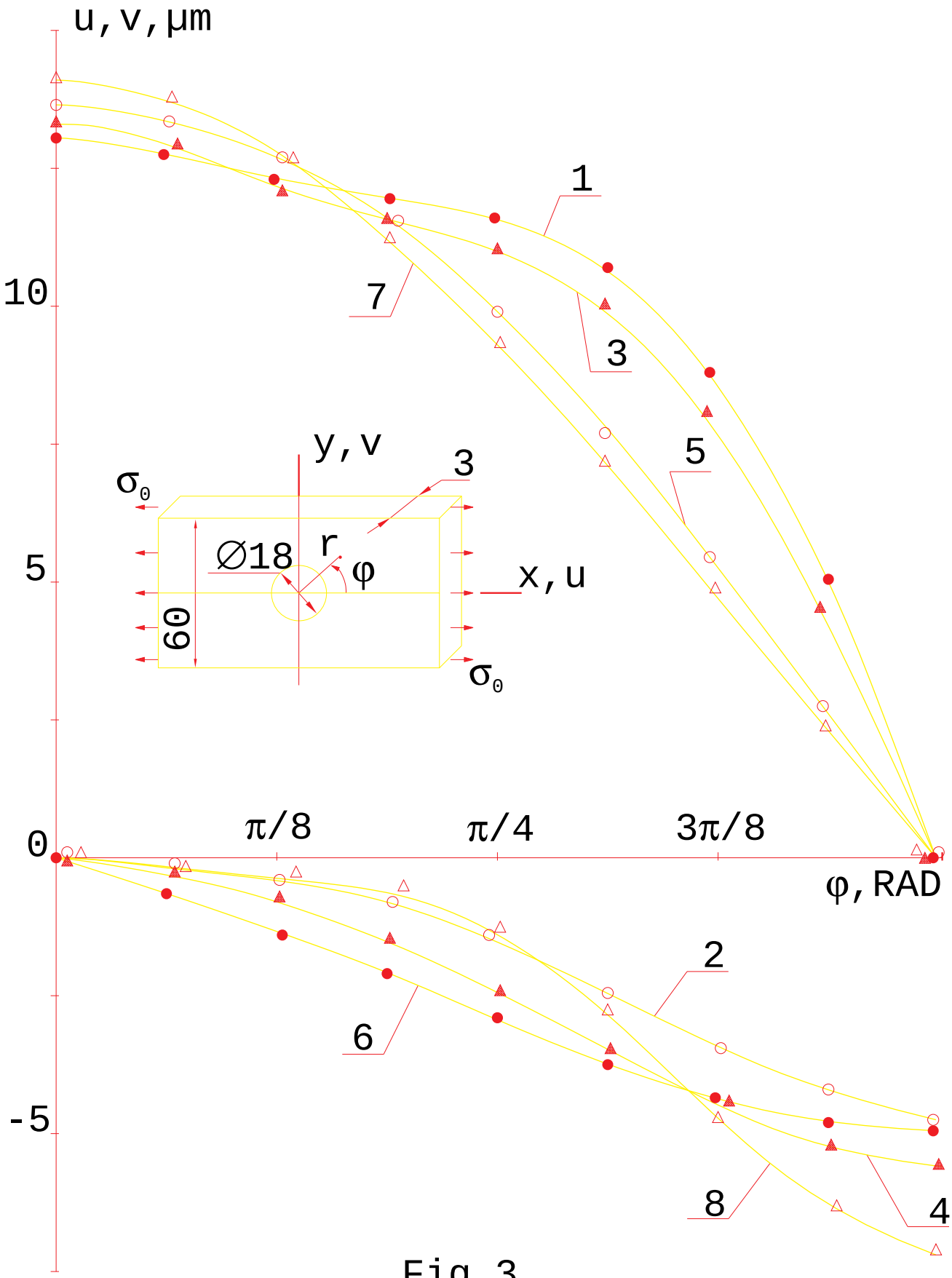

Fig.3.
In-plane Cartesian displacement component distributions around the hole in the plane specimen

Fig. 4 Distribution of the circumferential strain around the hole in the plane specimen

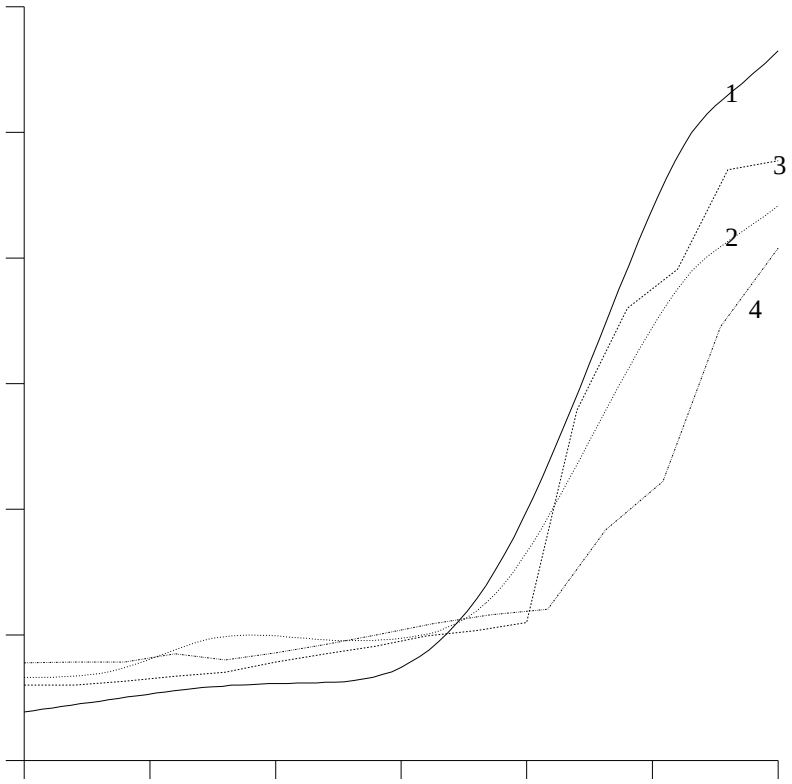

Maximum local strain vs net stress diagram

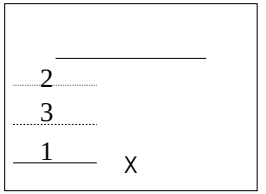

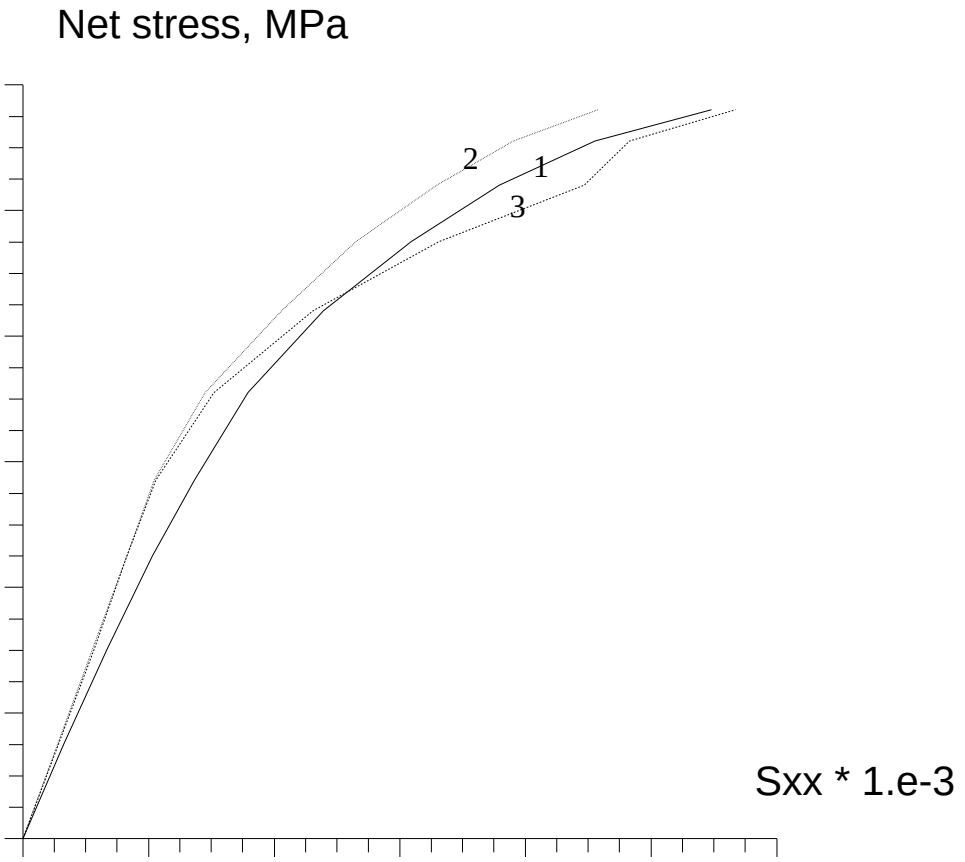

Fig. 6 Uniaxial strain vs stress diagram of the plane specimen material

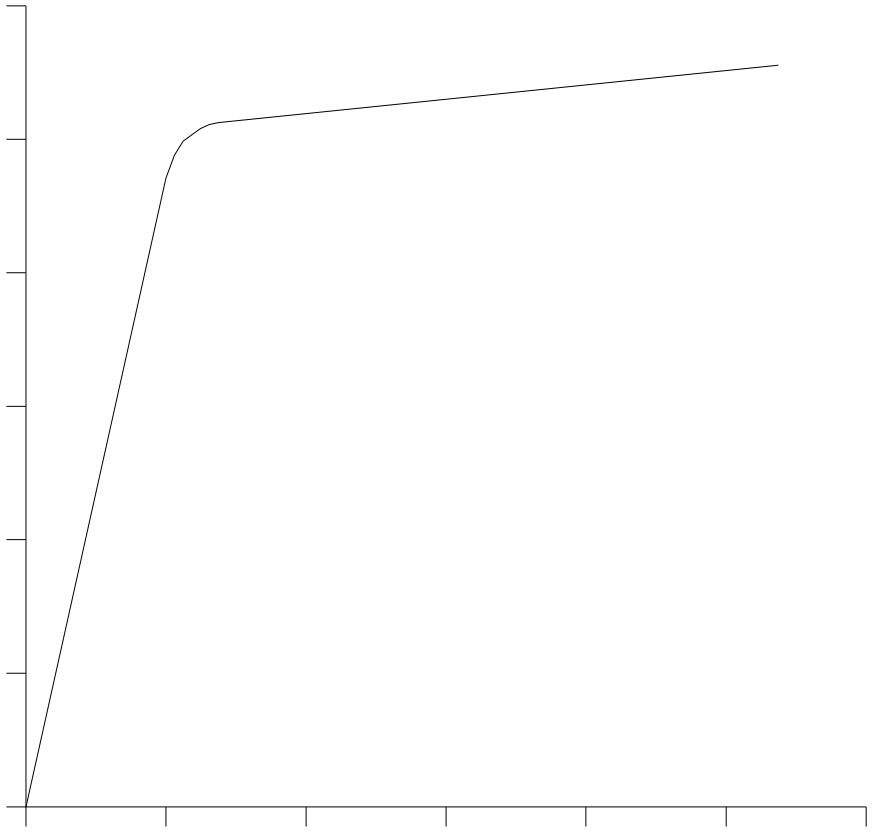

Distribution of total strain in the tension direction along central symmetry cross-section

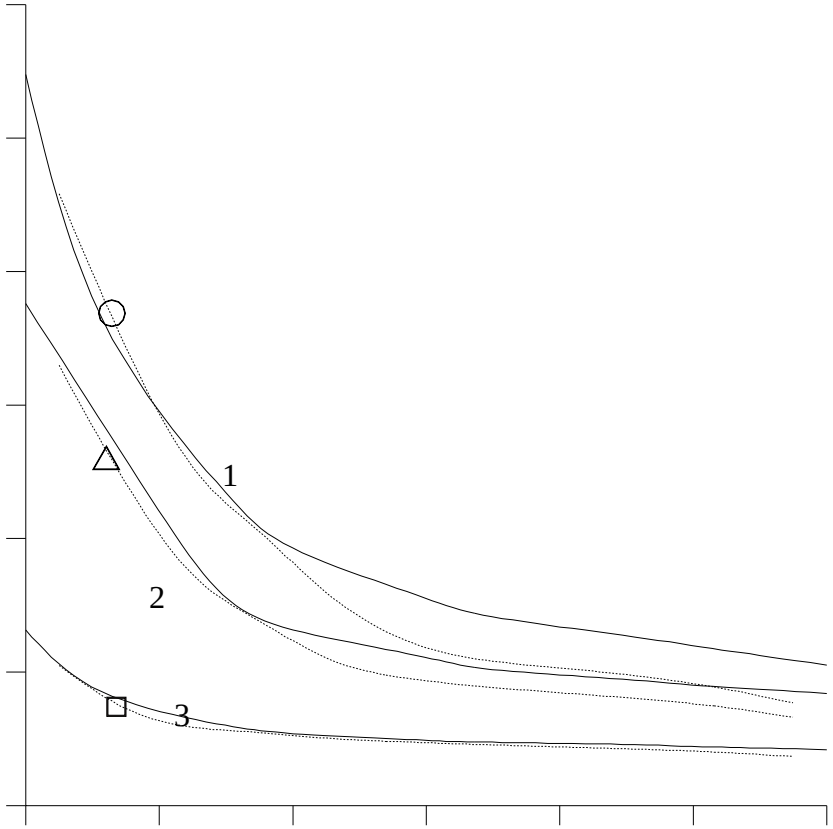

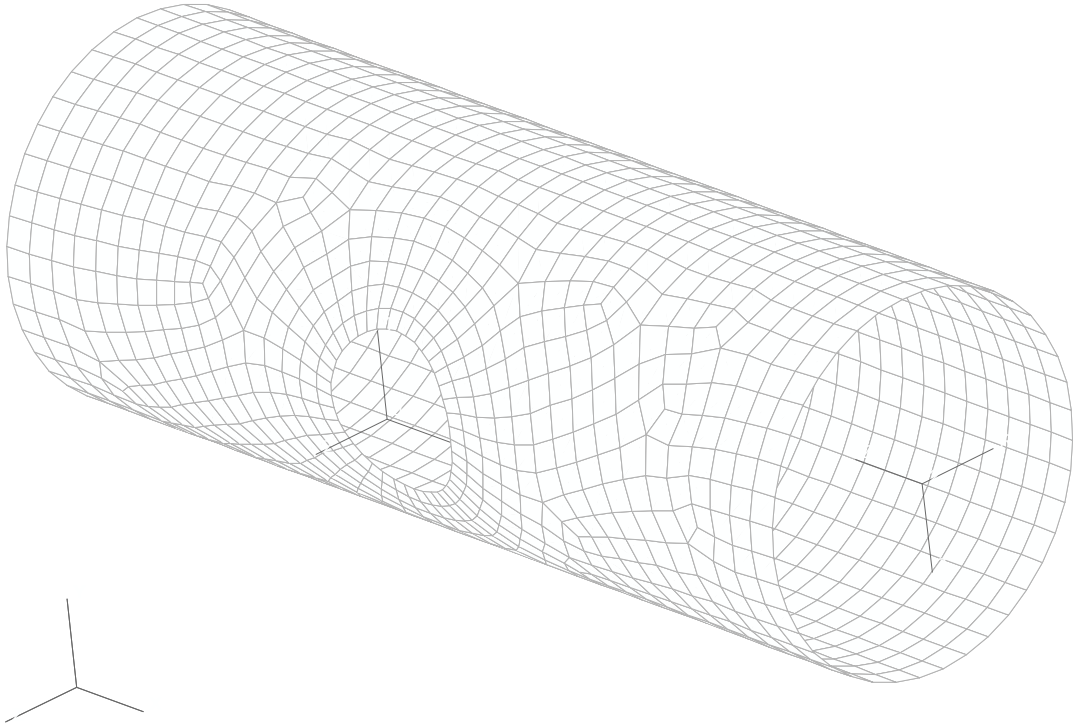

Fig 8. Scheme of shell with hole and finite element mesh used

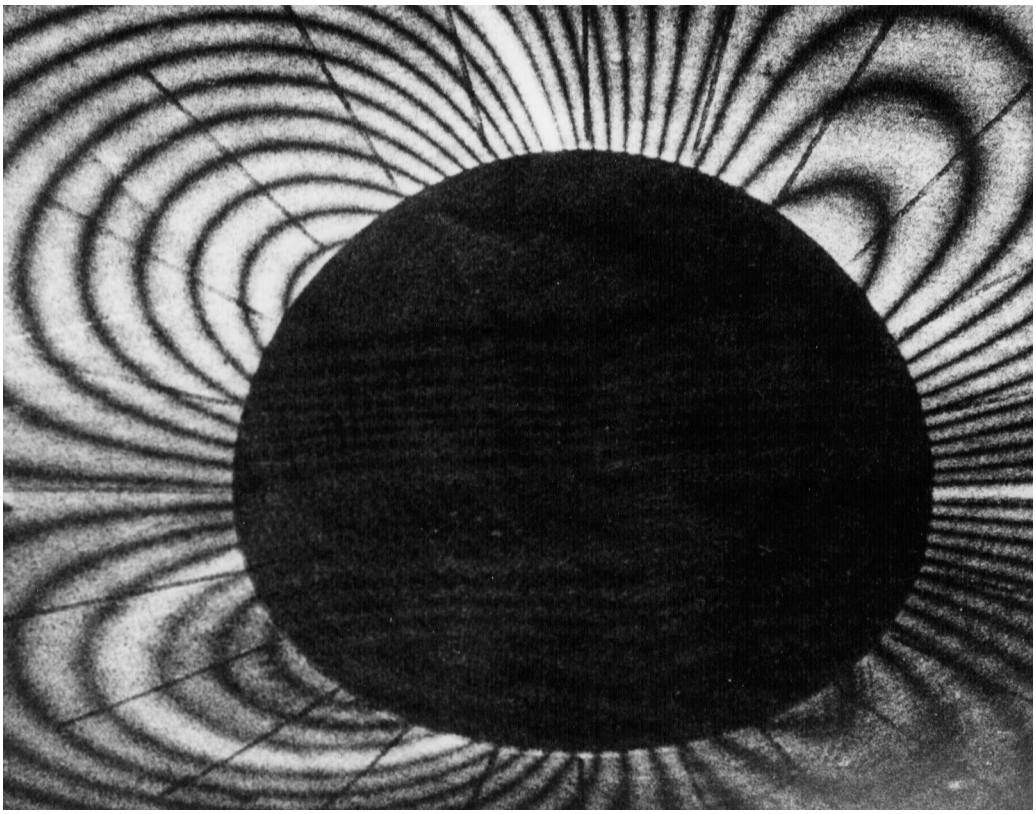

Fig. 9 Interferogram of the shell with hole subjected to a torsion

Fig.10 Distribution of the relative circumferential stress along the hole edge in the shell under torsion